

ORIGINAL RESEARCH PAPER

Synthesis of $\text{TiO}_2/\text{Fe}_3\text{O}_4/\text{MWCNT}$ Magnetic and Reusable Nanocomposite with High Photocatalytic Performance in the Removal of Colored Combinations from Water

Ahmad Vakili Tajareh, Hossein Ganjidoust*, Bita Ayati

Civil and Environmental Engineering Faculty, Tarbiat Modares University, Tehran, Iran

Received: 2019-04-23

Accepted: 2019-06-14

Published: 2019-08-01

ABSTRACT

In this study, $\text{TiO}_2/\text{Fe}_3\text{O}_4$ and $\text{TiO}_2/\text{Fe}_3\text{O}_4/\text{MWCNT}$ as new magnetic nano photocatalytic materials were synthesized. For this, TiO_2 nanoparticle was fixed on an inert surface by sonochemical method. X-ray Diffraction (XRD), scanning electron microscopy (SEM), UV-Vis diffuse reflectance spectroscopy (DRS), vibration sample magnetometry (VSM) were used to characterize the magnetic nanocomposites. SEM analysis indicated that TiO_2 and Fe_3O_4 nanoparticles have adhered to MWCNT. The ability of the nanocomposites to remove organic pollutants were investigated by photodegradation of Acid Red 14, Acid Blue 19, Reactive Red 77, and Methyl Orange dyes simulated conditions similar to sunlight. Furthermore, the removal efficiency of AR14 was investigated under direct sunlight irradiation, with an initial concentration of 50 mg/L by TiO_2 , $\text{TiO}_2/\text{Fe}_3\text{O}_4$ and $\text{TiO}_2/\text{Fe}_3\text{O}_4/\text{MWCNT}$ nanocatalysts were 89.83, 21.19 and 86.27, respectively. According to the results, addition of carbon nanotubes to the $\text{TiO}_2/\text{Fe}_3\text{O}_4$ magnetic nanocomposite increased the efficiency of AR14 photodegradation through change in energy gap visible waves and the scavenging role of carbon nanotubes. Also, The reusability of nanocomposites was assessed in five consecutive cycles of 6 hours, The results showed that after 5 cycles the degradation rate decreased only 7.79 %.

Keywords: Magnetic Nanocomposite, Photocatalytic, $\text{TiO}_2/\text{Fe}_3\text{O}_4/\text{MWCNT}$, Water Treatment, Xenon Light

How to cite this article

Vakili Tajareh A, Ganjidoust H, Ayati B. Synthesis of $\text{TiO}_2/\text{Fe}_3\text{O}_4/\text{MWCNT}$ Magnetic and Reusable Nanocomposite with High Photocatalytic Performance in the Removal of Colored Combinations from Water. J. Water Environ. Nanotechnol., 2019; 4(3): 198-212. DOI: 10.22090/jwent.2019.03.003

INTRODUCTION

Recently, in most studies, TiO_2 nanoparticles have been used for photocatalytic removal of pollutants from water because of their special photocatalytic properties. But the major disadvantages of the application of this nanoparticle in water treatment are the high cost of manufacturing nanoparticles and the probability of their occurrence in the environment. To overcome these problems, one of the suggested options is fixing materials on a static surface. However, this action reduces the number of active catalyst sites and consequently reduces the photocatalytic ability of these materials compared to non-supported nanocatalysts [1, 2].

Another promising solution for solving the problem of recycling nanoparticles in slurry systems is using magnetic nano-photocatalysts in the water treatment processes. When magnetic nanocomposites are used, they can be easily separated from the water by an external magnetic field [3]. Nanocomposites recycling will make the water purification processes with nanoparticles will be environment-friendly, more efficient and cost-effective [4].

So far, several magnetic nanocomposites have been used as photocatalyst for water purification, which in most cases follow a core-shell structure, consist of a formulated composite

* Corresponding Author Email: h-ganji@modares.ac.ir



with photocatalytic and magnetic nanomaterials. Usually, the internal core consists of magnetic elements such as iron, nickel, cobalt or their oxides, such as magnetite (Fe_3O_4), megamet ($\text{c-Fe}_2\text{O}_3$), cobalt ferrite (CoFe_2O_4) [5]. In addition, the shell is usually made with photocatalytic materials such as TiO_2 , ZnO , BiOCl and AgBr [6]. Recently, extensive studies have been carried out on the use of TiO_2 as coatings and SnO_2 and Fe_3O_4 oxides as a magnetic core [7]. Composition of TiO_2 photocatalytic nanoparticles with Fe_3O_4 superparamagnetic nanoparticles is not perfect because composition of these two nanoparticles together prevents the absorption of high-frequency light by TiO_2 nanoparticles. Also, the direct contact of the magnetic material and the TiO_2 nano photocatalyst causes the electron incompatibility issue [8, 9]. As a result, this phenomenon will cause a reduction in photocatalytic activity [10]. One solution to increase the photocatalytic activity of magnetic nanocomposites is doped them with another material such as SiO_2 nanoparticles [11], Ag [12] and C [13] to them, which were recently studied by researchers.

The main reason for the electron recombination in the nanocomposite is the proximity of energy level of Fe_3O_4 as conductor and the lowest unoccupied molecular orbital (LUMO) of the TiO_2 as semi-conductor transferred easily on the Fe_3O_4 nanoparticle surface and then will be recombined. According to studies, this issue can be solved by the addition of nanoparticles such as graphene or carbon nanotubes to the nanocomposite. According to Fig. 1, the excited electrons will be transferred on the Fe_3O_4 surface and then will be

transferred on MWCNT due to the lower energy of the MWCNT's work function.

According to studies, MWCNTs have a high ability to accept and scavenge electrons. Thus, by reducing the electron recombination the photocatalytic activity will increase [14, 15, 16]. In a study using TiO_2 - Fe_3O_4 /graphene nanocomposite, methyl blue dye photodegraded with 98.8% efficiency under UV light [17]. Also, the dye photodegraded with 100% efficiency under xenon light in another study [18]. Other similar studies have been done in the recent years consisting of photodegradation of RhB dye using of Graphene- TiO_2 - Fe_3O_4 [19], photodegradation of methyl Orange using of Fe-doped TiO_2 under visible light [20] and photodegradation of phenol using of Fe_3O_4 /C/ TiO_2 [21].

In the present study, the magnetic and photocatalytic TiO_2 / Fe_3O_4 /MWCNT nanocomposite was prepared using a simple, cost-effective and energy-efficient method to make nano photocatalyst materials with high photodegradation ability, reusable as well as the ability to be produced it industry. Other purposes of this study are to investigate the morphology, functional and photocatalytic activity of the nanocomposite in laboratory and real conditions.

EXPERIMENTAL

Materials

Carbon Nanotubes (MWCNTs) with an average diameter of 8 nm, length of 30 μm and purity of 95%. Iron (III) Chloride Hexahydrate ($\text{FeCl}_3 \cdot 6\text{H}_2\text{O}$), Iron (II) Sulfate Heptahydrate ($\text{FeSO}_4 \cdot 7\text{H}_2\text{O}$), Ammonium hydroxide (NH_4OH) and

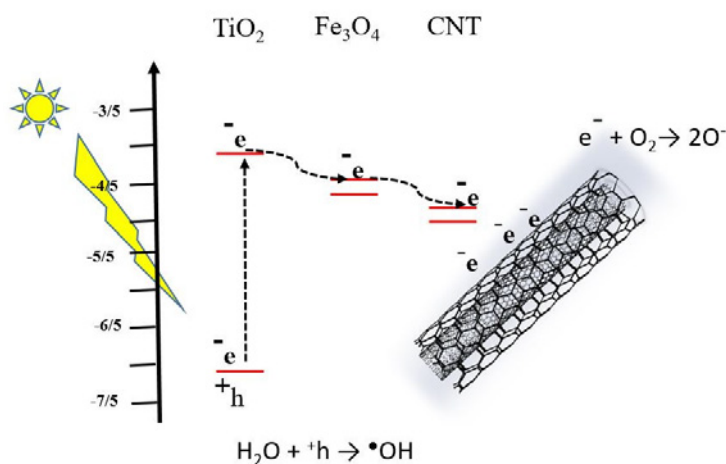


Fig. 1. Mechanism of Photocatalytic Performance Improvement in TiO_2 / Fe_3O_4 /MWCNT Nanocomposite

Hydrochloric acid were used in the synthesis of iron oxide nanoparticles. TiCl_4 , ethanol ($\text{CH}_3\text{CH}_2\text{OH}$), and Milli-Q water were used to prepare the TiO_2 nanoparticles and ammonium Sulfate ($(\text{NH}_4)_2\text{SO}_4$) was used for the preparation of $\text{Fe}_3\text{O}_4/\text{TiO}_2$ nanocomposites. Also, sulfuric acid (H_2SO_4) was used to activate the MWCNT carbon nanotubes. All chemicals were analytical grade and were purchased from Merck.

Synthesis of TiO_2

The TiO_2 anatase phase nanoparticles were synthesized using the hydrothermal method from TiCl_4 aqueous solution. For pure TiCl_4 and diluted it to 1 M was dissolved into the chloridric acid. In the following 100 ml of the TiCl_4 1 M solution was added to 200 ml of Milli-Q water. Drops of ammonium hydroxide (NH_4OH) were added slowly into the solution of titanium tetra chloride (TiCl_4) in order to adjust the pH value to 7 then the Milli-Q water was added again to increase the solution volume to 500 ml so as to adjust the concentration of Ti (IV) to 0.2 M. After stirring vigorously, the solution was made to settle for 12 hours. Then, the precipitate was centrifuged. The obtained sol was washed with deionized water to remove the chloride ions. Then, the precipitate was dried at 200°C to remove the absorbed water for 3 hours and finally amorphous TiO_2 was obtained. The obtained amorphous TiO_2 was calcinated at the temperatures of 300°C (heating rate $30^\circ\text{C}/\text{min}$) for 4 hours [22].

Synthesis of Fe_3O_4

3.01 g $\text{FeSO}_4 \cdot 7\text{H}_2\text{O}$ and 2.04 g $\text{FeCl}_3 \cdot 6\text{H}_2\text{O}$ were dissolved in deionized water. Both solutions then mixed together in an ultrasonic bath simultaneous nitrogen gas with a flow rate of 0.5 L min^{-1} and 1 atm pressure was introducing into the solution. The reaction process started when drops of 1M sodium hydroxide (NaOH) were added into the solution, then a black suspension appeared indicating the formation of magnetite. The precipitated nanomaterials were separated using the external magnetic bar and finally collected with a centrifuge and dried in Temperature at 80°C for one day [23].

Preparation of $\text{TiO}_2/\text{Fe}_3\text{O}_4$

At first 100 mg of prepared Fe_3O_4 nanoparticle was dispersed into the 200 mL deionized water. On other beakers, 1 g TiO_2 was dispersed into 100 mL of 0.02 M $(\text{NH}_4)_2\text{SO}_4$ and mixed with the magnetic nanoparticle suspension. The suspension was

sonicated for 30 minutes at room temperature then centrifuged at 4000 rpm to obtained solid material. The obtained solid was dried in oven for 18 hours, at a temperature of 100°C . the nanocomposite was obtained and ready for further experiments [24].

Surface modification of MWCNT

MWCNT were modified to introduce surface functional groups, e.g. -OH and -COOH. Briefly, 1.0 g MWCNT were added into 50 mL 1.7 M ammonium persulfate and 2.0 M H_2SO_4 mixture solution and was then placed in an ultrasonic bath for 3 hours. Upon completion, the mixture was kept in an oven at 50°C for 17 hours. Finally, the functionalized MWCNT was rinsed by 100 mL deionized water three times and dried in an oven at 60°C overnight [25].

Synthesis of $\text{TiO}_2/\text{Fe}_3\text{O}_4/\text{MWCNT}$ nanocomposite

In order to synthesis the electromagnetic and reusable $\text{TiO}_2/\text{Fe}_3\text{O}_4/\text{MWCNT}$ nanocomposite at first, the functionalized carbon nanotubes, in different weights 1, 2.5, 5, and 10 individually were dispersed into 100 mg ethanol ($\text{CH}_3\text{CH}_2\text{OH}$) then was placed in an ultrasonic bath for 30 minutes. In another container, 10 mg of the prepared Fe_3O_4 magnetic nanoparticles was dispersed in 200 ml of deionized water, then the solution was sonicated for 30 minutes, in the following the prepared Fe_3O_4 solutions were added to a nanotube carbon solution, as a result the nanoparticles iron covered the surface of carbon nanotubes. After washing the mixture with deionized water, it was placed inside the oven at 60°C for 24 hours to calcination procedure. In the next step, the prepared $\text{Fe}_3\text{O}_4/\text{MWCNT}$ nanocomposite was added to 200 mg deionized water and was sonicated for 30 minutes. In the last step, by using a non-homogeneous sonochemical method, the surface of the $\text{Fe}_3\text{O}_4/\text{MWCNT}$ nanocomposite was coated with TiO_2 nanoparticles (In Fig. 2, a schematic representation of how nanoparticles are deposited in $\text{TiO}_2/\text{Fe}_3\text{O}_4/\text{MWCNT}$ nanocomposites). It is known that Fe_3O_4 and TiO_2 have a different isoelectrostatics

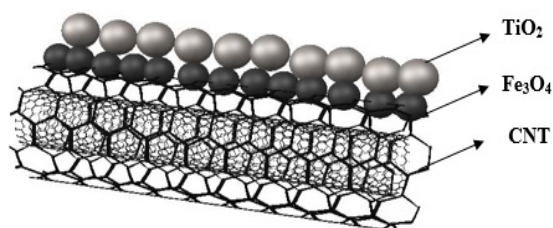


Fig. 2. Schematic image of $\text{TiO}_2/\text{Fe}_3\text{O}_4/\text{MWCNT}$ nanocomposite

point [26]. Based on the measurements of zeta potential, the surface charge of Fe_3O_4 changes from (+) to (-) at pH 8.5 while that of TiO_2 changes from (+) to (-) at about pH 5. At pH range above 5 and below 8, Fe_3O_4 possesses positive surface charge whereas TiO_2 has negative charge so that an attractive force would adhere to two particles together.

Characterizations

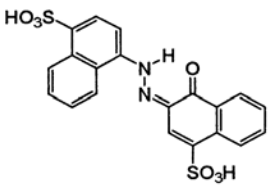
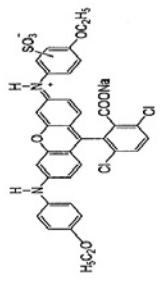
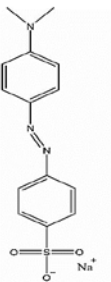
The crystal phase of the synthesized nanocomposites was characterized by X-ray diffraction (Philips X'Pert MPD). The elemental composition was studied by Dispersive X-ray Spectroscopy (EDS) analysis. The morphology and structure of the samples were investigated by Field Emission Scanning Electron Microscopy (FESEM, MIRA3, TESCAN), UV-Vis Diffuse Reflectance Spectra (DRS) of the samples were recorded on a UV-Vis spectrophotometer (Avaspec-2048-

TEC) with an integrating sphere attachment. Zeta potential of nanoparticle samples was investigated by Zeta potential analyzer (SZ-100Z, Horiba Jobin Jyovin). Spectra of the samples were measured using UV-Vis spectrophotometer (Hach - DR4000) in the range of 180 – 800 nm. Magnetometer (VSM) analysis was carried out on a Lakeshore V8 M7410 magnetometer. Ultrasonic bath, (Fungilab, UE-6SFD) to synthesis and disperse the nanomaterials.

Photo reactor and photocatalytic activity experiment

The photocatalytic activity of the synthesized nanocomposites was evaluated for four different dyes including Acid red 14, Methyl orange, Reactive Red 76 and Acid blue 19. Table 1, shows the specification of the evaluated dyes. To experiment the photocatalytic activity used a reactor (Fig. 3) consists of a glass reservoir of 600 cc and a cross-sectional area of 24/50 cm which surrounded by

Table 1. Specifications of tested dyes in photocatalytic removal by nanocomposites

Dye	Acid red 14 / Carmoisine	Acid Blue 19	Reactive Red 76	Methyl Orange
Chemical structure			unknown	
molecular formula	$\text{C}_{20}\text{H}_{12}\text{N}_2\text{Na}_2\text{O}_7\text{S}_2$	$\text{C}_{37}\text{H}_{31}\text{Cl}_2\text{N}_2\text{NaO}_8\text{S}$	unknown	$\text{C}_{14}\text{H}_{14}\text{N}_3\text{NaO}_3\text{S}$
Chemical category	Mono Azo	Xanthene class	Azo	Azo
Molecular Weight	502/44 grams	757/67 grams	unknown	327/33 grams
λ max (nm)	515	603	562	464
Uses	Uses as colors in wool, nylon, silk, leather, paper, printed nylon, the dye in aluminum Anadise	Use in the textile and leather industry	textile industry	the textile industry and laboratory for titration and acid detection

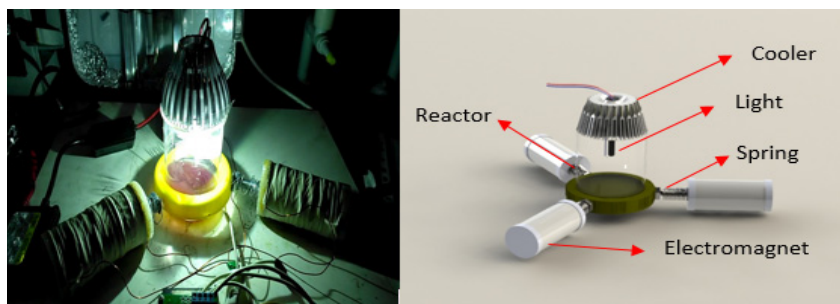


Fig. 3. Image of Photocatalytic Reactor and its Schematic

three electromagnets, to isolate and the maximum use of light, the reactor was embedded in an isolated optical box. For the visible light source, a 55 W Xenon lamp was used due to the closest radiation spectrum to sunlight [27].

In each experiment, 50 mg of nanocomposite was added to 50 mL dyes solution in the reactor at room temperature. Before irradiation, the suspension was stirred in the dark for 30 min to measurement the adsorption-. After the start of photocatalytic reaction in specified times, 5 mL of the suspension was taken and then the nanocomposite particles were separated by a magnetic to measurement dye concentration. Also, reusability of $\text{TiO}_2/\text{Fe}_3\text{O}_4/\text{MWCNT}$ nanocomposites was tested to evaluate the durability and stability, for this the nanocomposite was deposited and separated by a magnet within 1 minute, then washed with distilled water and dried at 60°C for 2 hours,

To ensure the accuracy of the results and to minimize the human error factor and equipment, the tests were performed with three times repeated and the means of data was used as results experiments.

RESULTS AND DISCUSSION

Determination of the optimal ratio of composition of $\text{TiO}_2/\text{Fe}_3\text{O}_4/\text{CNT}$

To investigate the effect of the compounds ratio on dye removal, $\text{TiO}_2/\text{Fe}_3\text{O}_4/\text{CNT}$ nanocomposites in four ratios (100: 10: 10), (100: 10: 5), (2.5: 100: 10) and (100: 10: 1) were made and investigated under visible light. According to Fig. 4, after 5.5 hours the amounts of dye removal efficiency

were 56.66, 60.27, 85.96 and 77.69%, respectively. The maximum efficiency was related to the nanocomposite with a ratio of 2.5: 100: 10.

DRS analysis results

Light absorption properties and energy gap on each of TiO_2 , $\text{TiO}_2/\text{Fe}_3\text{O}_4$, and $\text{TiO}_2/\text{Fe}_3\text{O}_4/\text{MWCNT}$ were studied by DRS analysis. The results of the DRS is shown in Fig. 5. At wavelength of 200 to 400 nm the TiO_2 nanoparticles have the highest light absorption whereas in $\text{TiO}_2/\text{Fe}_3\text{O}_4$ [28] and $\text{TiO}_2/\text{Fe}_3\text{O}_4/\text{MWCNT}$ composite the highest light absorption at a wavelength of 400 to 800 nm were observed.

In Fig. 6, the sharp edge gradient indicates the transition of electrons from the energy gap between the valence layer and the conduction layer, which is possible to determine the energy gap by using the equation 1 for each of the nanocomposites. The results are presented in Table 2.

$$(E) = h \cdot C / \lambda \quad (1)$$

In equation 1, $h = 6.626 \cdot 10^{-34}$ J/s (Planck's constant), C is the velocity of light in vacuum condition, which is equal to $3 \cdot 10^8$ m/s and λ is the wavelength of the light at the edge of the absorption.

According to Fig. 6, band gap value for the TiO_2 nanoparticles is 3.22 eV which after addition of Fe_3O_4 nanoparticles to TiO_2 band gap were shifted to the red and was measured in the range of 2.2 eV. It is also observed that with the addition of MWCNT, the energy gap shifted to blue (2.94 eV) that the highest absorption spectrum was in the visible range about 436 nm.

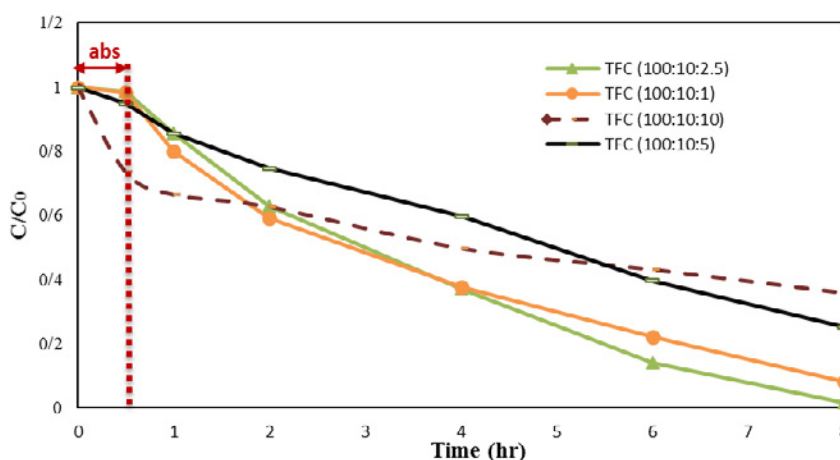
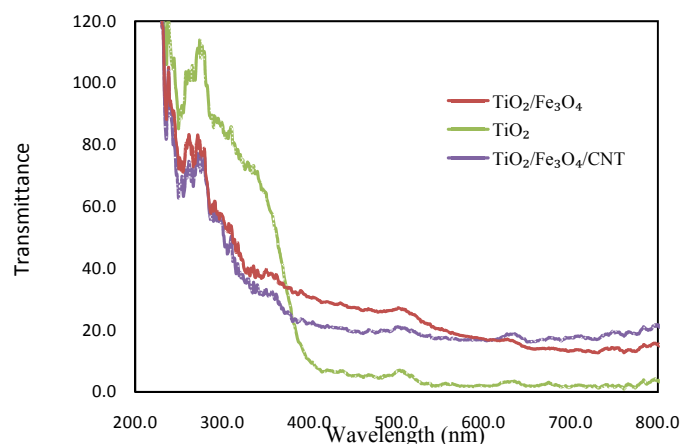
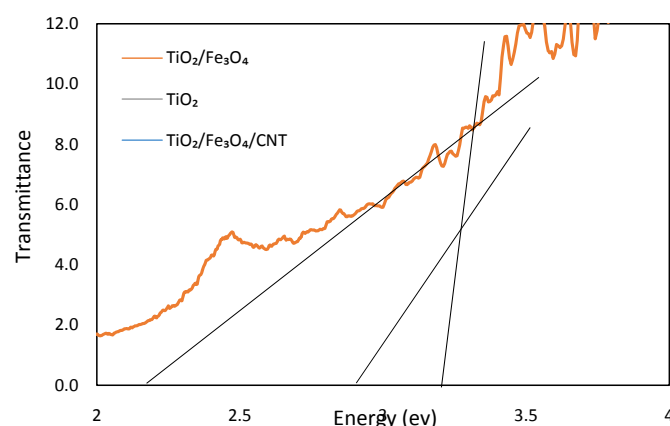


Fig. 4. Investigating the ratio of composition of $\text{TiO}_2/\text{Fe}_3\text{O}_4/\text{MWCNT}$
(Nanocomposite dosage = 0.5 g/L, dye concentration = 50 ppm, DO = 7/4 mg/L, pH= 7)

Table 2. The energy gap and the maximum absorption wavelength of TiO_2 , $\text{TiO}_2/\text{Fe}_3\text{O}_4$ and $\text{TiO}_2/\text{Fe}_3\text{O}_4/\text{MWCNT}$

Nanocatalyst	h (J/s)	C (m/s)	λ (nm)	E (ev)
TiO_2	$6/626 \times 10^{-34}$	3×10^{-8}	385	3/22
$\text{TiO}_2/\text{Fe}_3\text{O}_4$	$6/626 \times 10^{-34}$	3×10^{-8}	565	2.2
$\text{TiO}_2/\text{Fe}_3\text{O}_4/\text{MWCNT}$	$6/626 \times 10^{-34}$	3×10^{-8}	436	2/94

Fig. 5. The absorption spectra of each of TiO_2 , $\text{TiO}_2/\text{Fe}_3\text{O}_4$ and $\text{TiO}_2/\text{Fe}_3\text{O}_4/\text{MWCNT}$ nanomaterials by DRS analysisFig. 6. Determination of energy bases using the results of the DRS test for each TiO_2 , $\text{TiO}_2/\text{Fe}_3\text{O}_4$ and $\text{TiO}_2/\text{Fe}_3\text{O}_4/\text{MWCNT}$ nanomaterial

XRD analysis

XRD measurements were carried out to investigate the crystal identity of $\text{TiO}_2/\text{Fe}_3\text{O}_4$ and $\text{TiO}_2/\text{Fe}_3\text{O}_4/\text{MWCNT}$ nanocomposites. Fig. 7 shows the XRD pattern TiO_2 , $\text{TiO}_2/\text{Fe}_3\text{O}_4$, and $\text{TiO}_2/\text{Fe}_3\text{O}_4/\text{MWCNT}$. The diffraction peaks at $2\theta = 25.37^\circ$, 37.81° , 48.21° , 54.01° , 55.11° , 63.01° , 69.02° and 75.25° are determined. The presence of TiO_2 nanoparticles in the anatase phase [29]. In the $\text{TiO}_2/\text{Fe}_3\text{O}_4$ and $\text{TiO}_2/\text{Fe}_3\text{O}_4/\text{MWCNT}$ diffraction peaks at $2\theta = 30.21^\circ$, 35.51° , 43.31° , 53.21° , 57.21° and 63.01° indicate the presence of Fe_3O_4 superparamagnetic nanoparticles [30].

SEM and EDX analysis

FESEM and EDS tests were performed to investigate the morphology and ensure the formation of nanocomposites. In Fig. 8, FESEM images of Fe_3O_4 , MWCNT nanoparticles, $\text{TiO}_2/\text{Fe}_3\text{O}_4$, $\text{TiO}_2/\text{MWCNT}$, and $\text{TiO}_2/\text{Fe}_3\text{O}_4/\text{MWCNT}$ nanocomposite are presented.

The average diameter of the nanoparticles of iron oxide is between 14 to 35 nm (Fig. 8-a), and the average particle diameter in $\text{TiO}_2/\text{Fe}_3\text{O}_4$ nanocomposite is between 19 to 25 nm (Fig. 8-b). Compared to a similar study reported by Harifi et al. (2014) [31], they are of a lower average value,

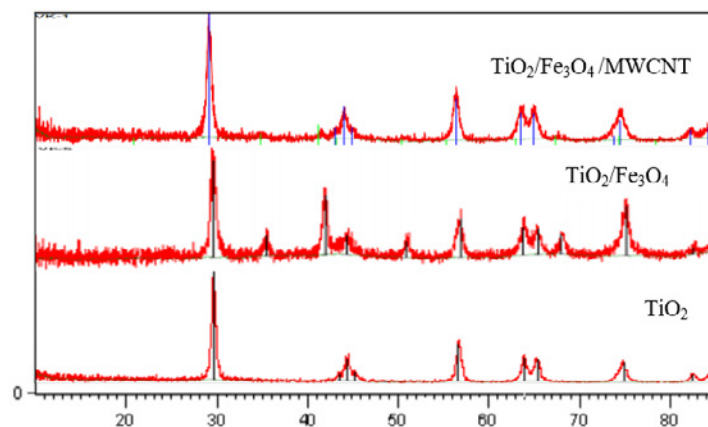


Fig. 7. XRD spectra of TiO_2 , $\text{TiO}_2/\text{Fe}_3\text{O}_4$ and $\text{TiO}_2/\text{Fe}_3\text{O}_4/\text{MWCNT}$

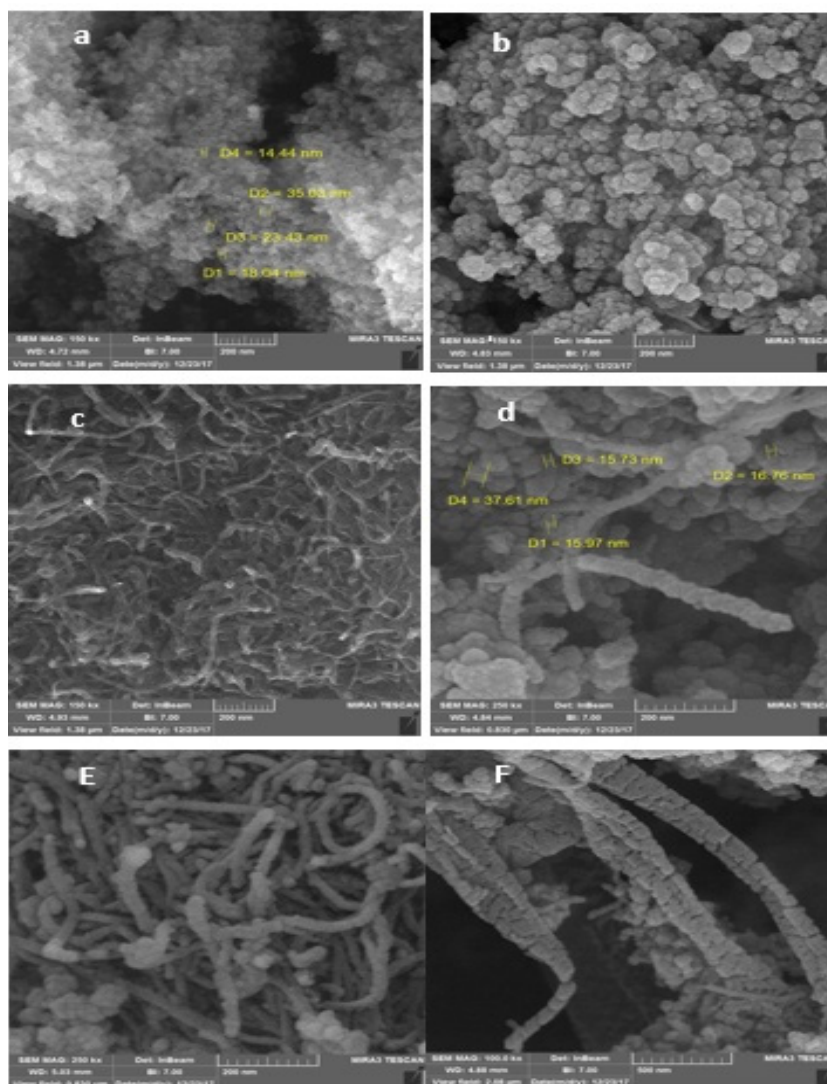


Fig. 8. FESEM images a) Fe_3O_4 nanoparticles b) $\text{TiO}_2/\text{Fe}_3\text{O}_4$ nanocomposite c) MWCNT d) $\text{TiO}_2/\text{MWCNT}$ e and f) $\text{TiO}_2/\text{Fe}_3\text{O}_4/\text{MWCNT}$

which indicates the high quality of nanocomposite production.

In Fig. 7, $\text{TiO}_2/\text{Fe}_3\text{O}_4/\text{MWCNT}$ nanocomposite FESEM images can be seen in two different parts, the particle size is in the nanoscale size and despite the presence of carbon nanotubes, there is not much accumulation and particles are separated, also is observed Fe_3O_4 and TiO_2 nanoparticles are well covered the carbon nanotubes. In Fig. 8-F, it is observed that the diameter of the nanotube has been increased, which can be due to the coating of two layers of nanoparticles. TiO_2 nanoparticles were bonded to the surface of the MWCNT also the nanoparticles themselves are almost continuously bonded so that there are no uncovered parts on the surface of the nanotubes.

The EDS analysis was performed to determine the ratio of particles in nanocomposite particles in optimal conditions. Fig. 9, shows the qualitative results of the EDS analysis that the presence of energy peaks of 4.56, 6.18 and 0.27 K_{ev} , respectively, indicate the presence of Ti, Fe and C elements in the nanocomposite. Also, in Table 3, the weight percent of each of the elements are provided. the weight percent of C, O, Ti and Fe elements were 5.48, 41.46, 46.84 and 22.6 percent respectively,

which is approximately equal to the ratio of nanocomposite in the specified state (100/10/2.5: $\text{TiO}_2/\text{Fe}_3\text{O}_4/\text{MWCNT}$).

Investigating the Magnetism of Nanocomposites

To determine the magnetic strength of the nanocomposite, the VSM analysis at room temperature was performed on Fe_3O_4 nanoparticles and $\text{TiO}_2/\text{Fe}_3\text{O}_4/\text{MWCNT}$ nanocomposites in weight ratio (2.5: 100: 10) and their magnetic curves were plotted, which can be seen in Figs. 10 and 11. The results show that Fe_3O_4 nanoparticles have a superparamagnetic property, and despite the low weight ratio of nanoparticles of Fe_3O_4 in the composition, the $\text{TiO}_2/\text{Fe}_3\text{O}_4/\text{MWCNT}$ nanocomposites were well-magnetized.

Photocatalysis activity of nanocomposites

To evaluate the photocatalytic degradation by the nanocomposite, the dye degradation in the specified conditions was investigated by $\text{Fe}_3\text{O}_4/\text{TiO}_2$ nanocomposite and TiO_2 nanoparticles, as shown in Fig. 12. The dye degradation efficiency by $\text{Fe}_3\text{O}_4/\text{TiO}_2/\text{MWCNT}$ was much higher than $\text{Fe}_3\text{O}_4/\text{TiO}_2$ nanocomposites and was equal to the efficiency by TiO_2 nanoparticles alone and slightly

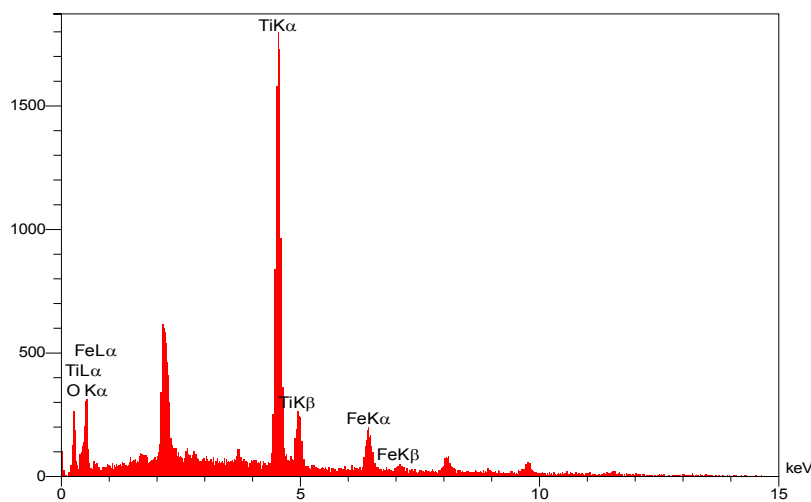
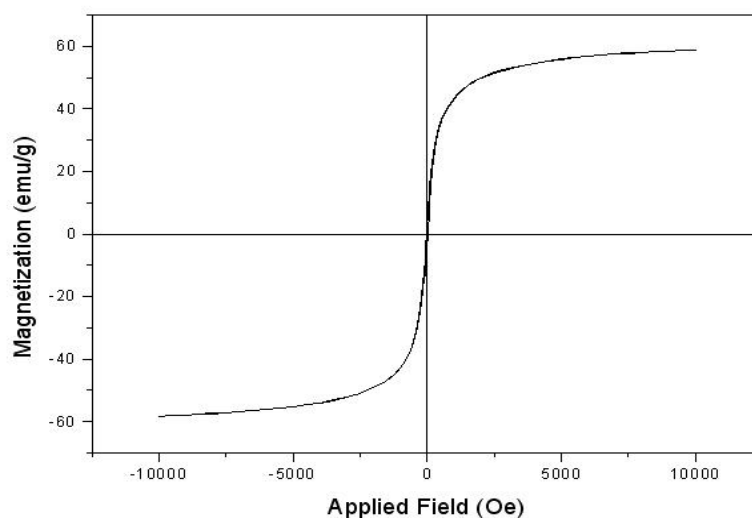
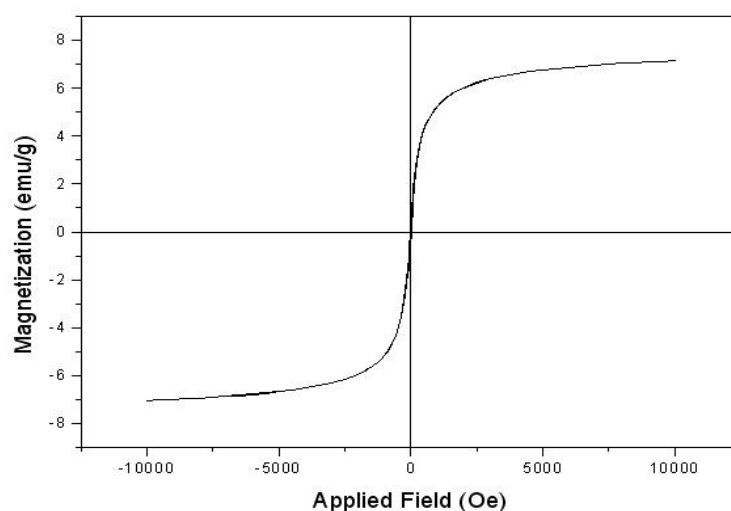


Fig. 9. Qualitative results obtained from the EDS of $\text{TiO}_2/\text{Fe}_3\text{O}_4/\text{MWCNT}$ nanocomposite

Table.3. Quantitative results obtained from EDS of $\text{TiO}_2/\text{Fe}_3\text{O}_4/\text{MWCNT}$

Elt	Line	Int	K	Kr	W%	A%	ZAF	Pk/Bg
C	Ka	29.4	0.0417	0.0237	5.48	11.03	0.4325	19.63
O	Ka	89.8	0.1294	0.0736	41.46	62.64	0.1775	58.71
Ti	Ka	406.1	0.7367	0.4189	46.84	23.64	0.8944	31.52
Fe	Ka	46.3	0.0923	0.0525	6.22	2.69	0.8434	6.18
			1.0000	0.5687	100.00	100.00		

Fig. 10. Magnetic intensity measurement curve of Fe_3O_4 nanoparticles at room temperatureFig. 11. Magnetic intensity measurement curve of $\text{TiO}_2/\text{Fe}_3\text{O}_4/\text{MWCNT}$ at room temperature

different in the elimination process.

An increase in the dye degradation efficiency by the nanocomposite could be due to the reduction of the energy gap caused by the MWCNT pegging to the TiO_2 nanoparticles or the scavenger role of MWCNT and accumulation of electrons on MWCNT particles and the prevention of recombination of the free hole in TiO_2 [32].

According to Fig. 12, we could say that $\text{Fe}_3\text{O}_4/\text{TiO}_2/\text{MWCNT}$ nanocomposites have higher initial absorption than TiO_2 nanoparticles alone, which can be due to the presence of MWCNTs that is an excellent absorbent of organic and inorganic materials [33].

Also initially, the start of the light emission to the reactor photodegradation rate by the TiO_2 nanoparticles is more than the $\text{Fe}_3\text{O}_4/\text{TiO}_2/\text{MWCNT}$ nanocomposite, but after a while, this difference disappears, partly because of the dye absorbed on the surface of the $\text{Fe}_3\text{O}_4/\text{TiO}_2/\text{MWCNT}$ nanocomposite which reduces photon absorption.

To further investigation of the photocatalytic activity of the nanocomposite, degradation of other dyes including acid blue 19, reactive red 77 and methyl orange were measured under optimal conditions; the results are shown in Fig. 13. The rate of degradation was measured after 4 hours

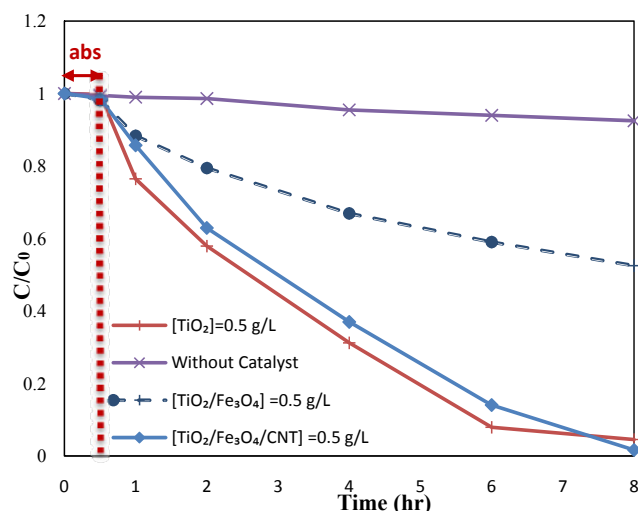


Fig. 12. The rate of removal of acid red 14 by TiO₂, TiO₂/Fe₃O₄ and TiO₂/Fe₃O₄/MWCNT (Nanocomposite dosage = 0.5 g/L, dye concentration = 50 ppm, DO = 7/4 mg/L, pH= 7)

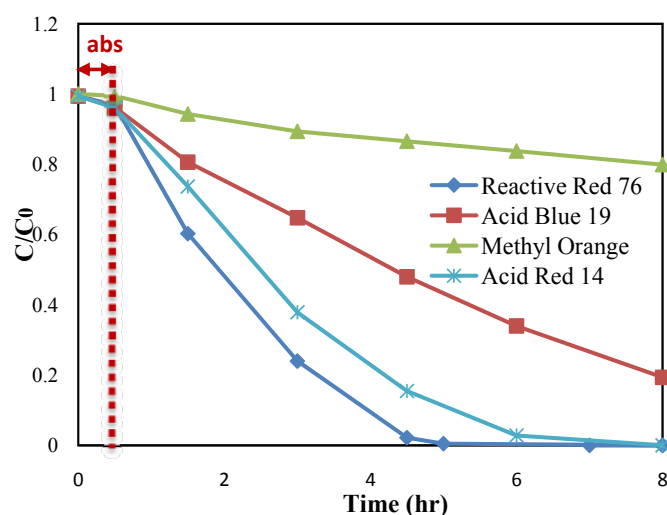


Fig. 13. Inset of removal of various dyes of methyl orange, reactive red 76 and acid blue 19 (Nanocomposite dosage = 0.5 g/L, dye concentration = 50 ppm, DO = 7/4 mg/L, pH= 7)

from the onset of light exposure for acid blue 19, reactive red 77, and methyl orange equal to 21.25, 97.87 and 13.44 percent, respectively. The results show that the nanocomposite is ineffective in the degradation of Methyl orange dye.

To find out this issue, the principal properties of the dye, as well as the degradation of dye by another nanoparticle, were investigated. The results are shown in Fig. 14.

In a study by Dorraj et al., 2017 [34], the degradation of Methyl Orange under xenon light

radiation and the use of TiO₂ nanoparticles were investigated, the efficiency less than 10% was reported. Also, Zhang et al., [35], study about the degradation of Methyl Orange by nanocomposite P25 TiO₂ (Degussa), the similar results and very low efficiency was reported again [36]. In the investigation of the degradation efficiency of methyl Orange dyes by TiO₂ and Fe₃O₄/TiO₂, the degradation rate after 4 hours was 19.04 and 19.02%, respectively.

To the structural analysis of the methyl orange dye

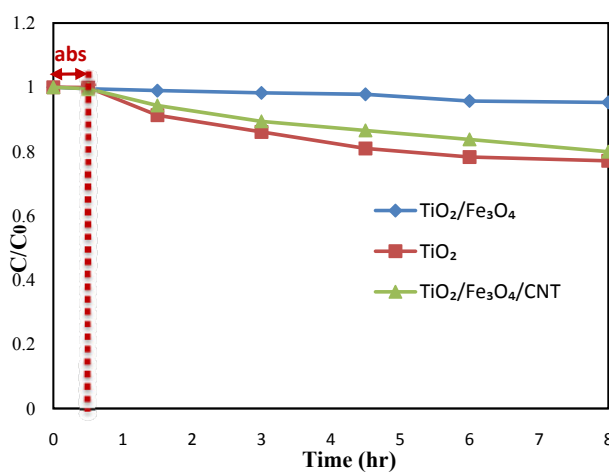


Fig. 14. Determination of methyl orange dye removal by TiO_2 and $\text{TiO}_2/\text{Fe}_3\text{O}_4$ (Nanocomposite dosage = 0.5 g/L, dye concentration = 50 ppm, DO = 7/4 mg/L, pH= 7)

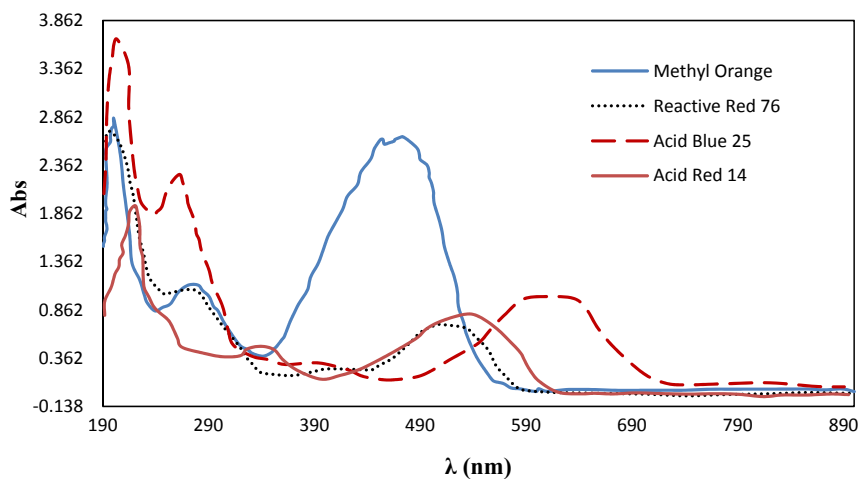


Fig. 15. Methyl orange spectrometry, Reactive Red 76, Acid Blue 15 and Acid Red 14 in light visible light and UV

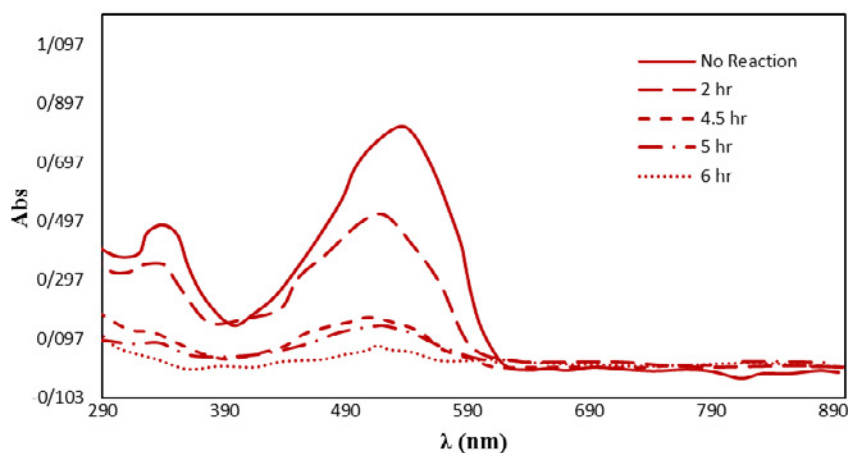


Fig. 16. UV-Vis spectra changes of red 14 during the photocatalytic reaction (Nanocomposite dosage = 0.5 g/L, dye concentration = 50 ppm, DO = 7/4 mg/L, pH= 7)

and its difference with another dye, the absorption spectra of acid red 14, acid blue 19, reactive red 77 and methyl orange were investigated. According to Fig. 15, its optical absorption was much higher than of acid red 14. Most of the photons are absorbed by dye. It will no longer be absorbed by photocatalyst to stimulate electrons. This can be attributed to the low dye degradation by the nanocomposite and the total photocatalytic reaction.

Investigation of the mechanism of dye removal

Fig. 16. Shows a typical time-dependent UV-Vis spectrum of AR14 solution during photoirradiation. The absorption peaks, corresponding to dye, diminished and finally disappeared under reaction which indicated that the dye had been degraded. The UV-Vis spectrum of AR14 mainly consisted of three well-resolved bands. They were 514, 322 and 220 nm, respectively. The lowest energy absorption band (514 nm) was assigned to the $n\text{-}\Pi^*$ transition of (-N=N-) group and the peak observed in ultraviolet spectra absorption was assigned to the $\Pi\text{-}\Pi^*$ related to naphthalene rings bonded. According to Fig. 16, adsorption values during photocatalytic reaction decreased and after 4 and 6 hours, minor and Major peak have disappeared, respectively which can be attributed to the collapse of azo bonds due to oxidation.

Investigation of photocatalytic properties of nanocomposite in real conditions under sunlight

The energy from sunlight is recognized as a sustainable, clean and free source, and the benefits of this sustainable energy source are essential.

One of the main goals of this research is the use of sunlight source for the degradation of water pollutants, so the rate and amount of pollutant removal under sunlight was investigated in real terms.

An experiment was conducted to investigate the efficiency of photodegradation of acid red 14 under sunlight on December 18 and 19, 2017, and in the geographical location of 3837845/51, 7219535/35 (Tarbiat Modares University, Tehran, Iran) for 8 hours and in optimal condition. According to the information extracted from the World Meteorological Site (<https://www.wmo.int>), the average cloudiness of the weather was 5 and the humidity was 36 percent. Also the intensity of sunlight was measured every hour, with an average of 280 W/m^2 . Results of the study of the removal efficiency of dye under direct sunlight are shown in Fig. 17. The dye removal efficiency after 6 hours under direct sunlight for $\text{TiO}_2/\text{Fe}_3\text{O}_4/\text{MWCNT}$, $\text{TiO}_2/\text{MWCNT}$, $\text{TiO}_2/\text{Fe}_3\text{O}_4$, and TiO_2 Nanocatalyst was 86.27, 76.88, 19.19 and 89.53 percent, respectively.

The result indicates that, the high removal efficiency of the dye by the $\text{TiO}_2/\text{Fe}_3\text{O}_4/\text{MWCNT}$ nanocomposite under sunlight. Which confirms the economics of the process of removing pollutants from water with nanocomposites.

Reusability of $\text{TiO}_2/\text{Fe}_3\text{O}_4/\text{MWCNT}$ nanocomposite

Sustainability and reusability of a photocatalyst is a major factor in its applicability because it will be very effective at the final cost of sewage treatment. Reusability of $\text{TiO}_2/\text{Fe}_3\text{O}_4/\text{MWCNT}$

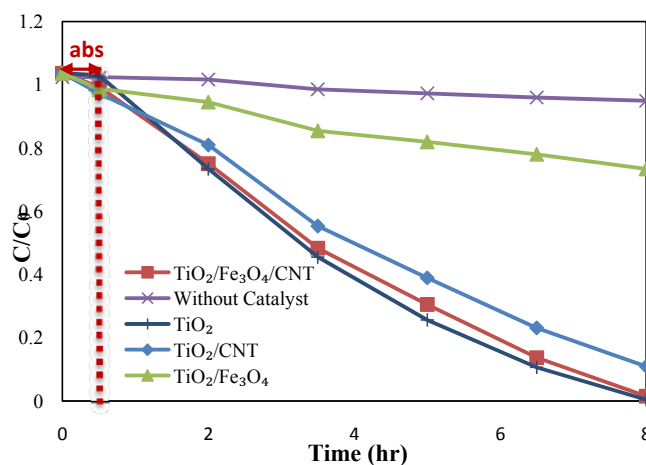


Fig. 17. Investigate of removal efficiency acid red 14 under sunlight
Nanocomposite dosage = 0.5 g/L, dye concentration = 50 ppm, DO = 7/4 mg/L, pH= 7))

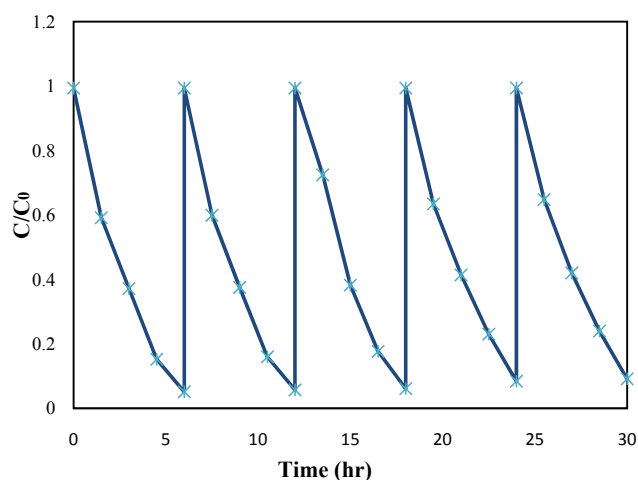


Fig. 18. Reusability of TiO₂/Fe₃O₄/MWCNT in 5 consecutive cycles
Nanocomposite dosage = 0.5 g/L, dye concentration = 50 ppm, DO = 7/4 mg/L, pH= 7))

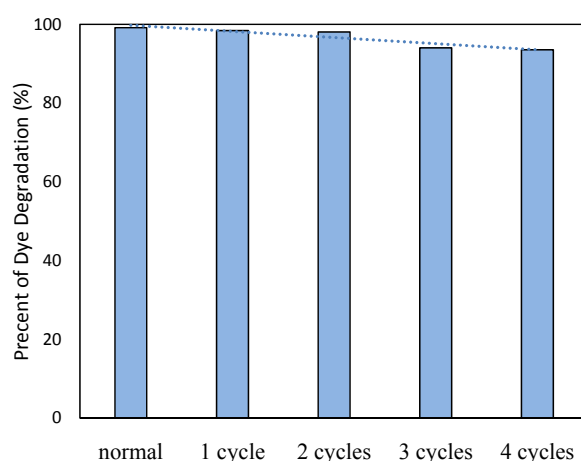


Fig. 19. The removal efficiency of acid red 14 after 6 hours in 5 consecutive cycles
Nanocomposite dosage = 0.5 g/L, dye concentration = 50 ppm, DO = 7/4 mg/L, pH= 7))

nanocomposites to evaluate the durability and stability under optimal conditions are presented in Fig. 18. According to the results after 3 cycles, there was no significant change in the efficiency of removing any of the dyes by the nanocomposite. For example, in the photocatalytic removal of AR14 after 4 hours, only 2.43% reduction was observed in the removal efficiency, but from period 4 to Then, the amount of reduction slightly increased after 4 hours compared to the first period, 7.79% reduction was observe in the dye removal efficiency, which could be due to various reasons, including loss of part of the nanocomposite during its recovery [29] or

remaining a portion of the pollutant on active site of nanocomposite surfaces [37] [38]. However, within 6 hours, light irradiation and in the fifth cycle 90.86% of the dye, was eliminated which demonstrates the high ability of nanocomposites to recycle and reuse, reducing the cost of removing dyes, solving the problem of its release in the environment, and hence increasing the chance of industrial use of nanocomposite. Also, in Fig. 19, the final efficiency of the removal of AR14 dye after 6 hours of light exposure as a result of 5 consecutive cycles is observed. Fig. 20 shows the difference between TiO₂/Fe₃O₄/MWCNT and TiO₂/MWCNT in sewage.

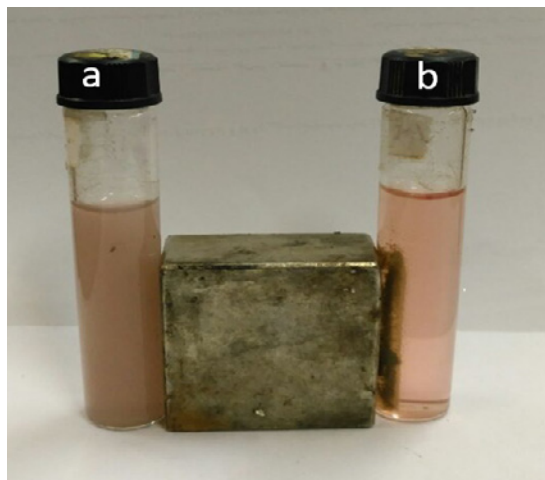


Fig. 20. a- Sewage containing $\text{TiO}_2/\text{MWCNT}$ nanoparticles
b- Sewage containing $\text{TiO}_2/\text{Fe}_3\text{O}_4/\text{MWCNT}$ magnetic nanocomposite

CONCLUSION

In this study, with a simple and inexpensive method, TiO_2 nanoparticles could be magnetically extracted by superparamagnetic Fe_3O_4 nanoparticles. Also, the addition of carbon nanotubes prevented the reduction of photocatalytic activity of nanocomposite, so that dye degradation during 6 hours under sunlight in optimum condition by TiO_2 alone, $\text{Fe}_3\text{O}_4/\text{TiO}_2$ and $\text{TiO}_2/\text{Fe}_3\text{O}_4/\text{CNT}$, was measured 89.53, 21.19 and 86., respectively. To investigate the application of nanocomposite in removal of others pollutants, the removal efficiency of MO, RR76 and AB19 dyes were measured 22.16, 99.51 and 66.02 respectively. Also, its reusability was investigated in 5 cycles that only 7.79% reduction in degradation efficiency was observed. According to the results, the stability of the solar source and the ability to recycle and reusability $\text{TiO}_2/\text{Fe}_3\text{O}_4/\text{CNT}$ nanocomposites was founded the nanocomposite is useful in removing non-biodegradable pollutants.

ACKNOWLEDGMENTS

The study was supported by a grant from the Tarbiat Modares University (TMU). The authors have no conflicts of interest to declare.

CONFLICTS OF INTEREST

There are no conflicts to declare.

REFERENCES

1. Zhou Q, Fang Z, Li J, Wang M. Applications of TiO_2 nanotube arrays in environmental and energy fields: A review. *Microporous and Mesoporous Materials*. 2015;202:22-35.
2. Udom I, Ram MK, Stefanakos EK, Hepp AF, Goswami DY. One dimensional- ZnO nanostructures: Synthesis, properties and environmental applications. *Materials Science in Semiconductor Processing*. 2013;16(6):2070-83.
3. Gómez-Pastora J, Dominguez S, Bringas E, Rivero MJ, Ortiz I, Dionysiou DD. Review and perspectives on the use of magnetic nanophotocatalysts (MNPCs) in water treatment. *Chemical Engineering Journal*. 2017;310:407-27.
4. Wang J, Yang J, Li X, Wang D, Wei B, Song H, et al. Preparation and photocatalytic properties of magnetically reusable $\text{Fe}_3\text{O}_4/\text{ZnO}$ core/shell nanoparticles. *Physica E: Low-dimensional Systems and Nanostructures*. 2016;75:66-71.
5. Linley S, Leshuk T, Gu FX. Magnetically Separable Water Treatment Technologies and their Role in Future Advanced Water Treatment: A Patent Review. *CLEAN - Soil, Air, Water*. 2013;41(12):1152-6.
6. Yao YR, Huang WZ, Zhou H, Zheng YF, Song XC. Self-assembly of dandelion-like $\text{Fe}_3\text{O}_4/\text{C}@\text{BiOCl}$ magnetic nanocomposites with excellent solar-driven photocatalytic properties. *Journal of Nanoparticle Research*. 2014;16(6).
7. Karunakaran C, SakthiRaadha S, Gomathisankar P. Photocatalytic and bactericidal activities of hydrothermally and sonochemically prepared $\text{Fe}_2\text{O}_3\text{-SnO}_2$ nanoparticles. *Materials Science in Semiconductor Processing*. 2013;16(3):818-24.
8. Fisli A, Saridewi R, Dewi SH, Gunlazuardi J. Preparation and Characterization of $\text{Fe}_3\text{O}_4/\text{TiO}_2$ Composites by Heteroagglomeration. *Advanced Materials Research*. 2012;626:131-7.
9. Mortazavi-Derazkola S, Salavati-Niasari M, Mazhari M-P, Khojasteh H, Hamadani M, Bagheri S. Magnetically separable $\text{Fe}_3\text{O}_4/\text{SiO}_2/\text{TiO}_2$ nanostructures supported by neodymium(III): fabrication and enhanced photocatalytic activity for degradation of organic pollution. *Journal of Materials Science: Materials in Electronics*. 2017;28(19):14271-81.
10. Zhang L, Wu Z, Chen L, Zhang L, Li X, Xu H, et al. Preparation of magnetic $\text{Fe}_3\text{O}_4/\text{TiO}_2/\text{Ag}$ composite microspheres with enhanced photocatalytic activity. *Solid State Sciences*. 2016;52:42-8.
11. Liu Y, Wan JF, Liu CT, Li YB. Fabrication of magnetic $\text{Fe}_3\text{O}_4/\text{C}/\text{TiO}_2$ composites with nanotube structure and enhanced photocatalytic activity. *Materials Science and Technology*. 2016;32(8):786-93.
12. Gad-Allah TA, Kato S, Satokawa S, Kojima T. Treatment of synthetic dyes wastewater utilizing a magnetically separable photocatalyst ($\text{TiO}_2/\text{SiO}_2/\text{Fe}_3\text{O}_4$): Parametric and kinetic studies. *Desalination*. 2009;244(1-3):1-11.
13. Cao M, Wang P, Ao Y, Wang C, Hou J, Qian J. Photocatalytic degradation of tetrabromobisphenol A by a magnetically separable graphene- TiO_2 composite photocatalyst: Mechanism and intermediates analysis. *Chemical Engineering Journal*. 2015;264:113-24.
14. Viskadourakis Z, Paramès ML, Conde O, Zervos M, Giapintzakis J. Very high thermoelectric power factor in a $\text{Fe}_3\text{O}_4/\text{SiO}_2/\text{p-type Si}(100)$ heterostructure. *Applied Physics Letters*. 2012;101(3):033505.
15. Jeyalakshmi V, Mahalakshmy R, Krishnamurthy KR, Viswanathan B. Photocatalytic Reduction of Carbon Dioxide by Water: A Step towards Sustainable Fuels and Chemicals. *Materials Science Forum*. 2012;734:1-62.

16. Shiraishi M, Ata M. Work function of carbon nanotubes. *Carbon*. 2001;39(12):1913-7.
17. Zhang P, Mo Z, Wang Y, Han L, Zhang C, Zhao G, et al. One-step hydrothermal synthesis of magnetic responsive TiO₂nanotubes/Fe₃O₄/graphene composites with desirable photocatalytic properties and reusability. *RSC Adv*. 2016;6(45):39348-55.
18. Li Z-Q, Wang H-L, Zi L-Y, Zhang J-J, Zhang Y-S. Preparation and photocatalytic performance of magnetic TiO₂-Fe₃O₄/graphene (RGO) composites under VIS-light irradiation. *Ceramics International*. 2015;41(9):10634-43.
19. Lin Y, Geng Z, Cai H, Ma L, Chen J, Zeng J, et al. Ternary Graphene-TiO₂-Fe₃O₄ Nanocomposite as a Recollectable Photocatalyst with Enhanced Durability. *European Journal of Inorganic Chemistry*. 2012;2012(28):4439-44.
20. Ghorbanpour, M., & Feizi, A. (2019). Iron-doped TiO₂ Catalysts with Photocatalytic Activity. *Journal of Water and Environmental Nanotechnology*, 4(1), 60-66.
21. Liu Y, Wan JF, Liu CT, Li YB. Fabrication of magnetic Fe₃O₄/C/TiO₂composites with nanotube structure and enhanced photocatalytic activity. *Materials Science and Technology*. 2016;32(8):786-93.
22. Ahmed, B. O., Al Bedry, G., Ibrahim, Y., & Eassa, N. (2017). Preparation of High Quality TiO₂ Nanoparticles using TiCl₄. *Journal of Basic and Applied Science*.
23. Ghasemi, M., Mashhadi, S., Azimi-Amin, J. (2018). Fe₃O₄/AC nanocomposite as a novel nano adsorbent for effective removal of cationic dye: Process optimization based on Taguchi design method, kinetics, equilibrium and thermodynamics. *Journal of Water and Environmental Nanotechnology*, 3(4), 321-336.
24. Fisli A, Saridewi R, Dewi SH, Gunlazuardi J. Preparation and Characterization of Fe₃O₄/TiO₂ Composites by Heteroagglomeration. *Advanced Materials Research*. 2012;626:131-7.
25. Ji T, Tu R, Mu L, Lu X, Zhu J. Structurally tuning microwave absorption of core/shell structured CNT/polyaniline catalysts for energy efficient saccharide-HMF conversion. *Applied Catalysis B: Environmental*. 2018;220:581-8.
26. Clavel, G. (2009). Magnetic impurities in nanostructured materials (Doctoral dissertation, Universidade de Aveiro (Portugal)).
27. Martin, D. (2007). A practical guide to machine vision lighting. *Midwest Sales and Support Manager, Adv Illum*2007, 1-3.
28. Chen P, Cai Y, Wang J, Wang K, Tao Y, Xue J, et al. Preparation of protonized titanate nanotubes/Fe₃O₄/TiO₂ ternary composites and dye self-sensitization for visible-light-driven photodegradation of Rhodamine B. *Powder Technology*. 2018;326:272-80.
29. Hu J, Wang H, Dong F, Wu Z. A new strategy for utilization of NIR from solar energy—Promotion effect generated from photothermal effect of Fe₃O₄@SiO₂ for photocatalytic oxidation of NO. *Applied Catalysis B: Environmental*. 2017;204:584-92.
30. Shen J, Zhou Y, Huang J, Zhu Y, Zhu J, Yang X, et al. In-situ SERS monitoring of reaction catalyzed by multifunctional Fe₃O₄@TiO₂@Ag-Au microspheres. *Applied Catalysis B: Environmental*. 2017;205:11-8.
31. Harifi T, Montazer M. A novel magnetic reusable nanocomposite with enhanced photocatalytic activities for dye degradation. *Separation and Purification Technology*. 2014;134:210-9.
32. Woan K, Pyrgiotakis G, Sigmund W. Photocatalytic Carbon-Nanotube-TiO₂Composites. *Advanced Materials*. 2009;21(21):2233-9.
33. Karthika V, Arumugam A. Synthesis and characterization of MWCNT/TiO₂/Au nanocomposite for photocatalytic and antimicrobial activity. *IET Nanobiotechnology*. 2017;11(1):113-8.
34. Dorraj M, Alizadeh M, Sairi NA, Basirun WJ, Goh BT, Woi PM, et al. Enhanced visible light photocatalytic activity of copper-doped titanium oxide–zinc oxide heterojunction for methyl orange degradation. *Applied Surface Science*. 2017;414:251-61.
35. Zhang L, Zhao Y, Zhong L, Wang Y, Chai S, Yang T, et al. Cu₂S-Cu-TiO₂ mesoporous carbon composites for the degradation of high concentration of methyl orange under visible light. *Applied Surface Science*. 2017;422:1093-101.
36. Han C, Ge L, Chen C, Li Y, Xiao X, Zhang Y, et al. Novel visible light induced Co₃O₄-g-C₃N₄ heterojunction photocatalysts for efficient degradation of methyl orange. *Applied Catalysis B: Environmental*. 2014;147:546-53.
37. Chen, D., & Ray, A. K. (1999). Photocatalytic kinetics of phenol and its derivatives over UV irradiated TiO₂. *Applied Catalysis B: Environmental*, 23(2), 143-157.
38. Liu X, Zhang Q, Yu B, Wu R, Mai J, Wang R, et al. Preparation of Fe₃O₄/TiO₂/C Nanocomposites and Their Application in Fenton-Like Catalysis for Dye Decoloration. *Catalysts*. 2016;6(9):146.